Simple-Source Model for Military Jet Noise

Jessica Morgan

A senior thesis submitted to the faculty of
Brigham Young University
in partial fulfillment of the requirements for the degree of

Bachelor of Science

Kent L. Gee, Advisor

Department of Physics and Astronomy

Brigham Young University

April 2011

ABSTRACT

Simple-Source Model for Military Jet Noise

Jessica Morgan
Department of Physics and Astronomy
Bachelor of Science

This study explores an alternative approach using a semi-empirical equivalent simple-source model to analyze and characterize the turbulence-induced aeroacoustic sources from military jet aircraft. Initially the model is a single point source located above a hard plane such that the locations of destructive interference from its mirror image matched the measured interference nulls. This provides useful information about the location of the dominant noise source region from the jet. The model then develops into a superposition of Rayleigh-distributed line arrays of uncorrelated and correlated monopoles. The model is tested on an extensive set of acoustic data taken on an F-22 Raptor. Although the model's line source characteristics are developed using data from only one measurement plane, it is able to accurately reproduce the radiation at other measurement planes. This equivalent line source matches the current prevailing theory that the sideline radiation is largely due to uncorrelated noise, whereas the correlated sources dominate downstream. In addition, the semi-empirical, simple-source model results corroborate the theory that the peak source location moves upstream with increasing frequency and lower engine conditions.

Keywords: Jet Noise, Simple-source Model, Equivalent Model

ACKNOWLEDGMENTS

I would like to thank everyone who has supported me in my educational endeavors. Thank you Dr. Gee for giving me a research project and dedicating so much time to my success. Thank you Dr. Neilsen for patiently teaching and helping me with how to use your code and correcting this thesis. Thank you Alan Wall for helping me with my code and answering all my random questions. Thank you David Krueger being so cheerful all the time. Thank you for my parents for encouraging me to pursue my dreams and getting an education.

Contents

List of Figures

Chapter 1

Introduction

1.1 Motivation

Jet-powered military aircraft produce large amounts of noise. The major risks and drawbacks of jet noise are the reduction of military stealth, hearing loss of ground personnel and noise pollution to the surrounding community. Large amounts of aircraft noise has been a concern since the mass construction of jet engines for the first jet-fighter aircraft began at the end of World War II [1]. In the late 1940s, research began to determine the sources and characteristics of jet noise and possible methods of reducing it.

Military jets have come a long way from the Messerschmitt Me 263 in World War II to the modern F-22 Raptor as jet technology continues to advance. Engineers are constantly working to improve jet engines and aircraft designs to make them more powerful, faster, stealthier, and lighter. Changing the design of jet engines, alters its noise characteristics. Jet noise research needs to remain in step with jet aircraft progression.

Jet noise research focuses on trying to understand and characterize the sources of jet noise. The turbulent nature of the jet exhaust plume complicates this entire endeavor. Additionally, desirable

acoustical measurements are limited due to the heat and intensity of the jet plume. However, over the past 60 years jet noise research has produced a body of knowledge concerning jet noise, but there is still much to learn.

1.2 Prevalent Theory of Jet Noise

Currently, the most prominent theory of jet noise indicates that there are two main sources of noise in a jet's exhaust plume: 1) directional large-scale turbulence structures (LSS) and 2) omni-directional fine-scale turbulence structures (FSS) [2]. A significant amount of research has investigated the connection between these dominant turbulence structures and the actual dominant sound radiation patterns. Several studies have yielded key information about the directivity and apparent location of noise sources in the plume. By studying vast data bases of jet noise, Tam has developed an empirical model that fits the main features of the LSS and FSS.

LSS and FSS come from two different regions of the jet plume. Small turbulence eddies, FSS, form at the nozzle and grow as they propagate downstream into LSS. There are still FSS within the LSS and are distributed throughout the jet plume. However, the dominate region of LSS is downstream. The FSS radiate omni-directionally contributing mostly to the sideline radiation of the jet, directly perpendicular to the jet plume. On the other hand, the LSS become coherent as they form downstream. In a coherent source each component radiates with a fixed phase difference. The components of the coherent source produce a constructive and deconstructive interference pattern. The resulting radiation pattern from the LSS is focused in one direction indicative of a directional source.

The directivity of LSS, or angle of prominent radiation, is one of the dominate features of jet noise [3]. The directivity radiation pattern is evident in far-field measurements which show the angle of primary sound radiation. The angle of radiation is measured with the aft, or front, of the

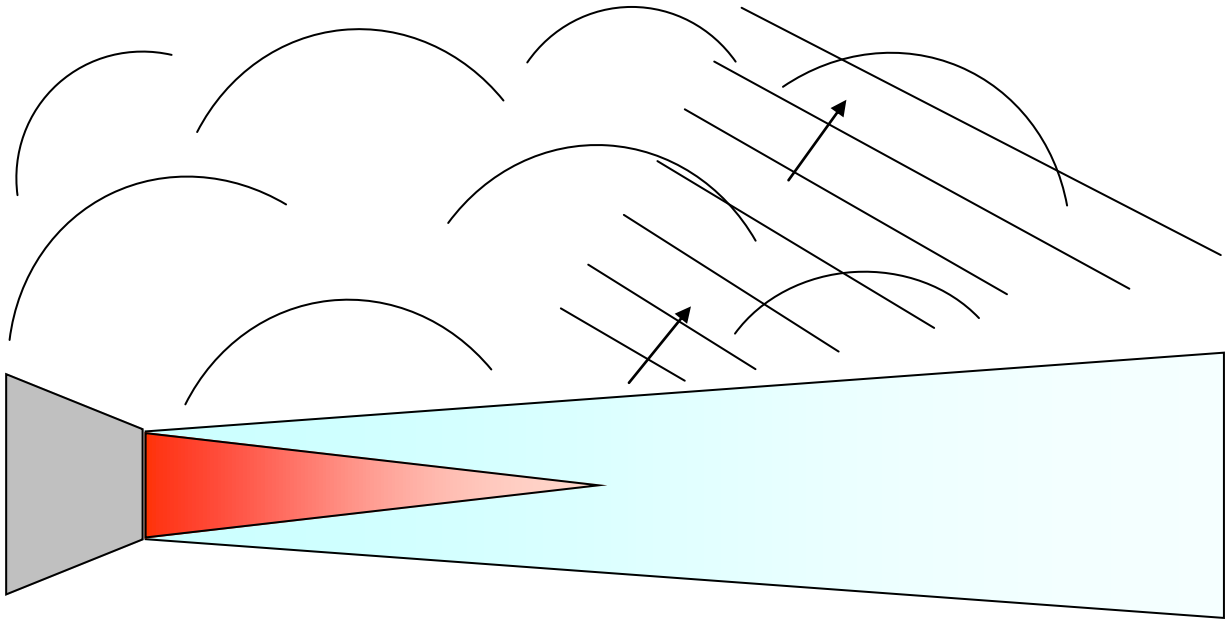

Figure 1.1 Fine-scale turbulence structure radiate omni-directional and large scale turbulence radiates is directional.

jet being zero degrees. The angle of sound radiation varies with engine powers and frequency. In general it has been found that higher engine powers radiate at shallower angles then the lower engine powers. Also higher frequencies radiate at shallower angles than lower frequencies.

When designing a model to simulate jet noises, it is important that the model can replicate this directivity radiation pattern. A coherent line array of sources has a similar effect of being able to steer sound in a specific direction. Such steering is only possible if the sources of sound are spatially distributed and does not occur for a point source.

Another dominate feature of jet noise is the apparent source location. Research indicates that the origin of peak sound radiation moves upstream as frequency increases [1] [4] [5]. The lower frequency sound radiates from the downstream direction of the jet plume, while the most prominent higher frequency sound radiates from close to the nozzle of the jet. Schlinker et. al. show in Fig. 11 b) that the spatial distribution of source strength according to frequency [4]. This shows that

the apparent origin of the lower frequencies are very spread out far downstream while the higher frequencies appear to originate in a dense area close to the nozzle. This suggests an asymmetric amplitude distribution of the sources in the spatially distributed line array of sources.

In addition to insights gained about directivity and apparent source location, analysis of jet noise data led to Tam and colleagues developing an empirical model of jet noise. This empirical model is known as the two source model because it uses two similarity spectra to simulate the properties of the observed jet noise radiation spectra. The two similarity spectra describe the LSS and FSS sound radiation spectra. Tam's G similarity spectra represents the sound dominated by FSS. The second similarity spectra, F, corresponds to the characteristics of the LSS. Both the F and G spectra fit together to make Tam's two source model of jet noise [2].

1.3 Techniques of Jet Noise Analysis

There are several different approaches to analyzing jet noise sources. These approaches fit into three different areas: measurement based, computational model and analytical modeling. Each of these uses a different component of jet noise research to model the sources of jet noise.

Ideally, it is best to use measured data to determine the source. There are several different measurement-based techniques. Some common measurement techniques are near-field acoustical holography (NAH) and beamforming. NAH takes a plane of acoustical measurements and propagates them in towards the jet plume to determine the source. NAH requires huge amounts of measured data and has quite a few assumptions build in. Typically, NAH is used to only propagate a few centimeters, but for jet noise applications it needs to be propagated several meters. One of the main difficulties in NAH is accounting for the evanescent waves decaying away from the source. NAH is very useful in reconstructing measurement planes close to the source, but it is difficult to execute. The other common measurement-based technique, beamforming, has a different

approach and uses measurements from a line array of microphones to determine the source location [3]. It uses the time delay of the radiated sound arriving at each adjacent microphone to figure out the angle that the noise is coming from. This is used to determine the peak source location. Beamforming is limited in the information that it provides. It gives the noise radiation relative to each angle off the jet plume, which is not the same as the overall noise radiation pattern. While these methods are very useful for analyzing acoustical data, they have their limitations.

Computational models are based on the fluid dynamics of the jet flow. These methods use Navier-Stokes equations for fluid flow to model the turbulence in the jet plume. The movement of the fluid in the jet plume is then coupled with the surrounding air to determine the radiated sound. One of the founders of jet noise research, Lighthill, took this approach to modeling jet noise [1] [6]. Lilley and Ffowes-William have made significant contributions to this model [1]. Despite the continuing improvements to this model, the turbulent nature of the jet plume makes this approach very difficult and computationally strenuous.

Analytical models use both measured data and known jet noise characteristics to determine the sources. Purely analytical models strive to predict sound radiation from the underlying equations of the physical process. However, it is more common to use a semi-empirical model that is partially based on measured data. Holste uses an equivalent source model and matches it to the measured data in order to predict the overall sound radiation instead of analyzing the source [7]. This method is useful for combining experimental data with known jet noise models. An analytical model method assumes that the model applies to the data. This method can still be very computationally difficult depending on the equivalent source or model chosen.

The purpose of this paper is to explore the plausibility of an alternative method of analyzing jet noise using a semi-empirical, equivalent simple source model. The major assumption is that a collection of simple sources can model the noise radiation of the complex structure in the jet plume, which makes it far simpler than previous models. This approach yields an equivalent

Figure 1.2 The jet strapped down to the runway with a rig of microphones to take data.

source distribution that best matches the measured acoustical data from a supersonic jet. The model consists of only simple (point) sources. The resulting source distribution is compared to previous theory of jet noise and may provide useful physical insight into jet noise.

1.4 Full-scale Experiment

1.4.1 F-22 Data Set-up

Before I joined the group, the jet noise research group at Brigham Young University took extensive noise measurements on an F-22 Raptor at Holloman Air Force Base in the summer of 2009. The group use a patch-and-scan method to make acoustical measurements in the near field of the jet. Measurements were made as close as the instruments allow. The jet was strapped down to the cement runway.

Figure 1.2 shows the set up of the jet with a microphone array taking measurements. The

Figure 1.3 A close up of the rig; a rectangular 5 by 18 microphone array. The rig is movable along a track.

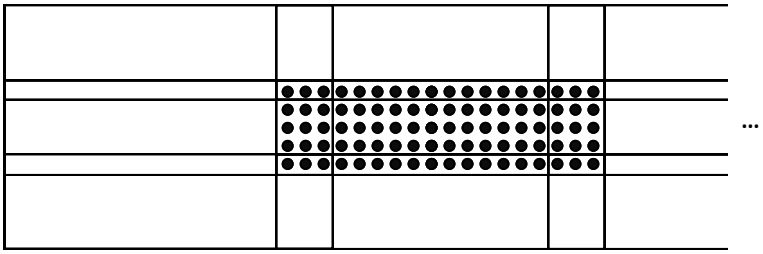

Figure 1.4 The schematic shows the location of the microphones in the array at one position. The other rectangles represent the 3 microphone overall as the rig is moved horizontally downstream and one microphone overlap as the rig is moved vertically.

patch-and-scan method uses multiple scans from a rectangular 5 by 18 microphone array to patch together a single measurement plane. Fig. 1.3 shows a close up photo of the microphone array. The microphone array slides along a track to all the measurement locations. The track is visible in Fig. 1.2 and Fig. 1.3. The microphone array is also adjustable in the vertical direction, it is set at three different heights with a one microphone overlap. Each microphone is set 15.2 cm (6 in) apart.

Figure 1.4 demonstrates how all the microphone array locations are pieced together. Each dot represents one microphone in a single scan location. The boxes show the location of adjacent measurement scan locations and how the microphone locations overlap in each direction.

The track, which the microphone array is on, can be moved to give multiple measurement planes. A single measurement plane is a series of adjacent microphone array measurements patched together. Fig. 1.5, shows the measurement locations. The red triangles along the track indicate the center of the the microphone array for subsequent measurement positions. The measurement planes of interest for this study are plane 1, plane 2 and plane 4. Plane 1 is parallel to the shear layer of the jet plume and 4.097 meters away. Measurement plane 2 is also parallel to the shear layer of the jet plume and 5.604 meters away. Data along both measurement plane 1 and 2 are taken at three heights and ten horizontal positions. Measurement plane 4 is an arc of ten degree increments, 22.9 meters away from the peak source location.

For every microphone array position in Fig. 1.5, measurements are taken at four different engine powers. The F-22 Raptor runs at engine powers labeled idle, intermediate, military and afterburner (AB). These are listed in order from idle being the least powerful to afterburner being the engine running at full power. The data set contains sound measurements for every engine condition at each measurement location at multiple heights. This is the most extensive, densest and closest experiment ever done on a high-performance jet. For more information on the experimental setup and measurement locations refer to Alan Wall's paper, "Near-field noise measurements of a high-performance military jet aircraft."

1.4.2 Experimental Measurements

While the microphones in the experiment record the time waveform of the sound pressure, the analysis of the sound field is carried out in the frequency domain. A Fourier transform on the data yields the frequency spectrum of the sound field. When the frequency spectra of the scans of

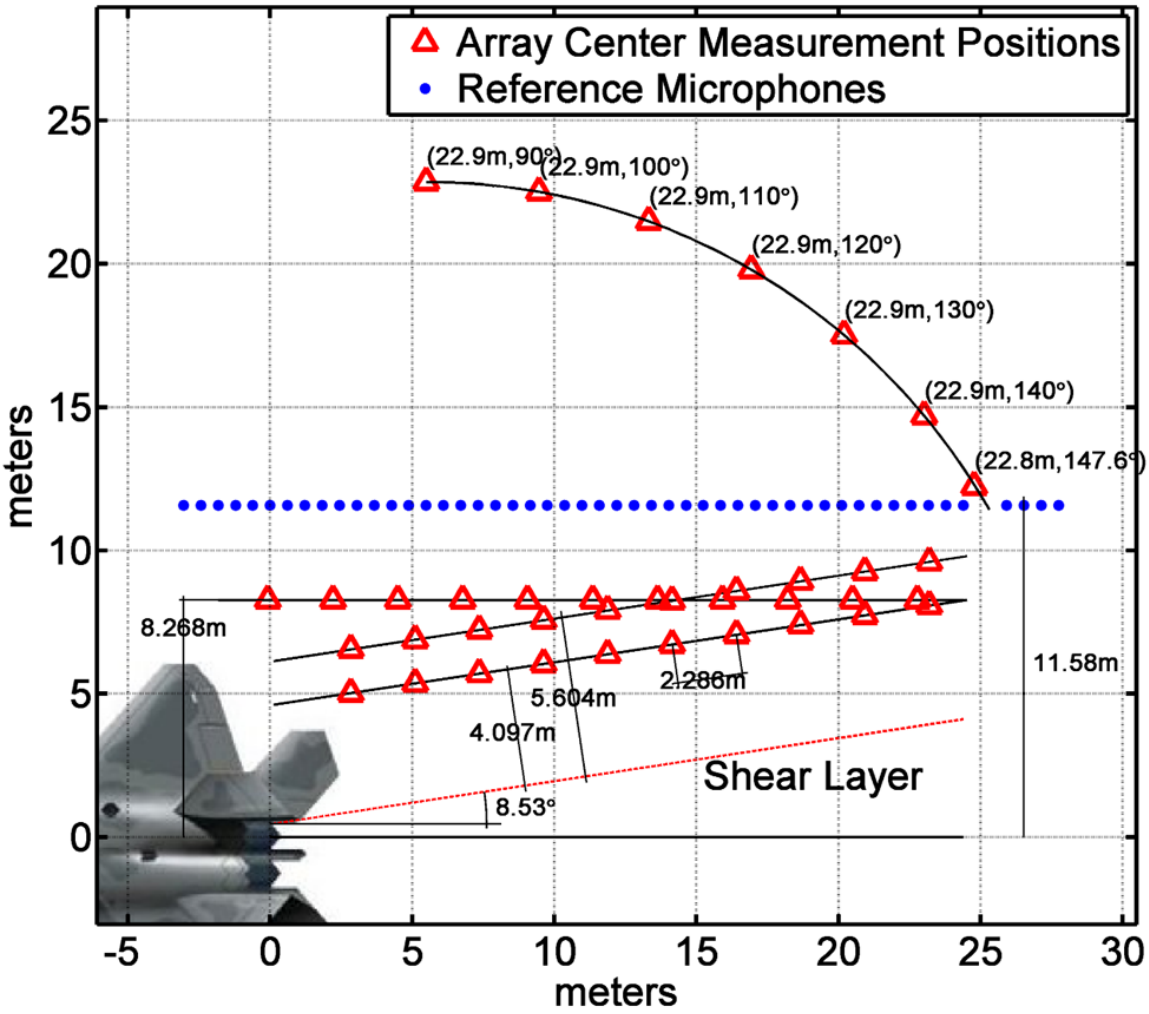

Figure 1.5 The experimental set up for taking acoustical measurements of an F-22 Raptor. The triangle mark each measurement location for the microphone array.

the F-22 data set are overlapped, as shown in Fig. reffig:rigrid, it produces a large 2 by 23 meter snapshot of the sound radiation for each frequency. Figs. reffig:df- reffig:dfp1 show a sampling of the acoustical data taken on the F-22 raptor. The plots show the sound pressure level (SPL) in dB:

$$SPL = 20\log_{10}\left(\frac{P(f)}{P_{ref}}\right), \tag{1.1}$$

where P_{ref} is 20e-5.

Figure 1.6 shows the sound radiation for four different frequencies at measurement plane 2 at the afterburner engine power. The frequencies are a) 150 Hz, b) 315 Hz, c) 795 Hz and d) 1245 Hz. Some inherent characteristics of jet noise are evident when comparing the different frequencies. First, the lower frequencies' peak levels are much further downstream than the higher

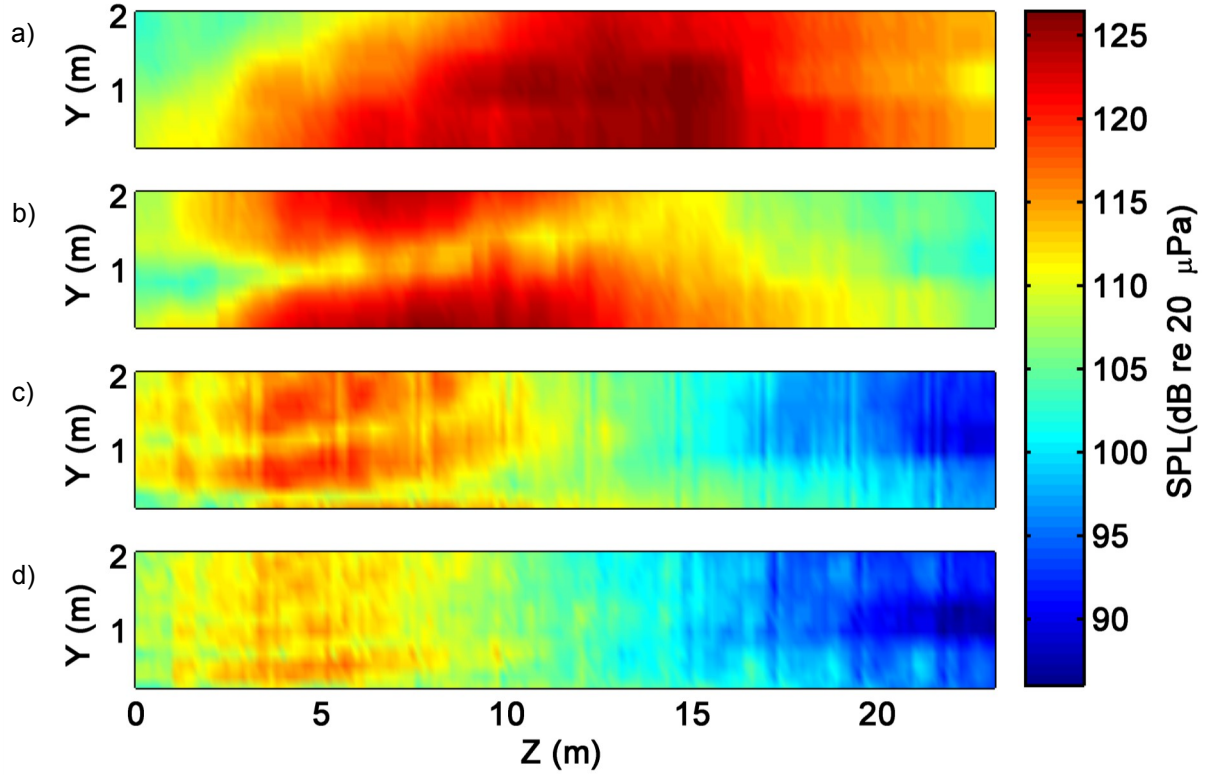

Figure 1.6 Acoustical data from the F-22 at measurement plane 2 distance 5.6 meters from the shear layer and afterburner engine condition a) 150 Hz, b) 315 Hz, c) 795 Hz, and d) 1245 Hz.

frequencies. This corresponds with the expectation that the peak radiation source shifts upstream closer to the nozzle as frequency increases. Additionally, the sound radiation at 150 Hz is much louder than at 1245 Hz. The majority of the total sound radiation comes from the lower frequencies that are centered downstream. Another prominent feature is the dip in SPL that runs horizontally through the data. These are nulls due to the interference between the direct sound and the ground reflections. At higher frequencies, the wavelength is shorter meaning that there are more nulls crossing through the plane of measurement. These plots show the basic trends of how the jet noise depends on frequency.

Figure 1.7 shows the sound field of the same four frequencies at AB, but closer to the source at measurement plane 1. For all of the frequencies the peak sound location moved upstream compared

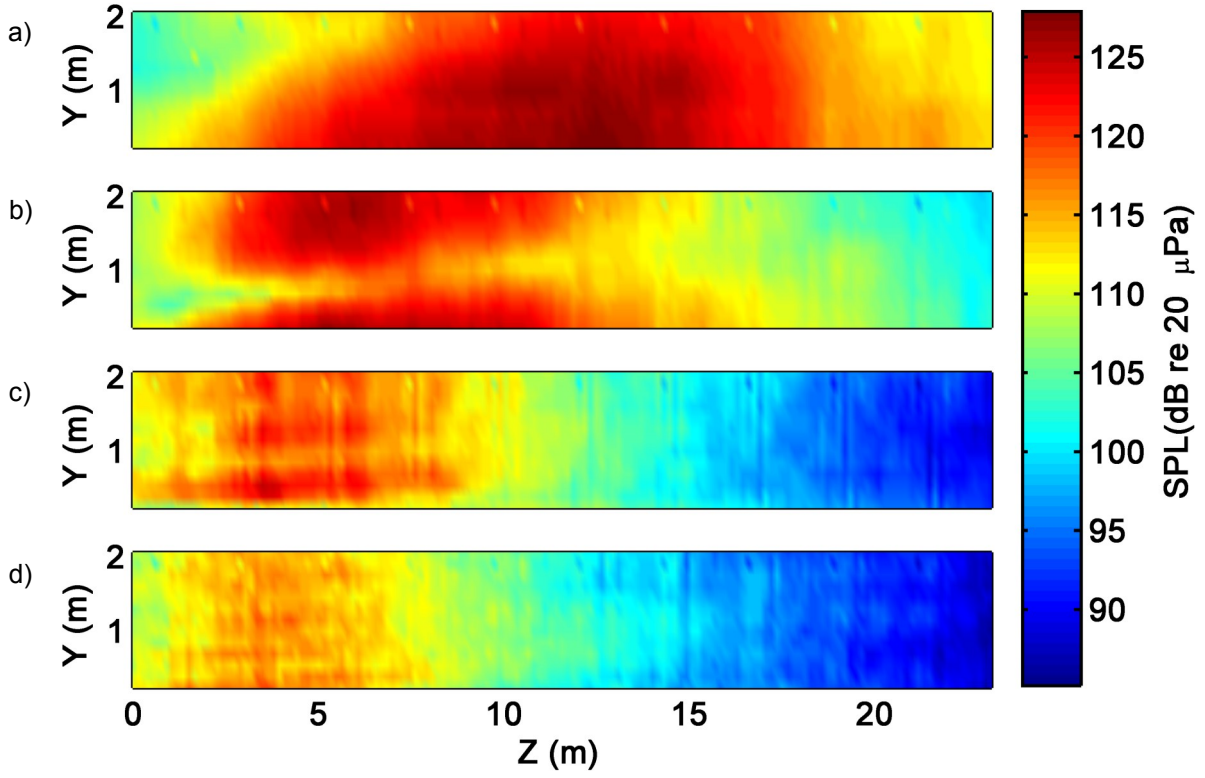

Figure 1.7 Acoustical data from the F-22 at measurement plane 1 distance 4.1 meters from the shear layer and afterburner engine condition a) 150 Hz, b) 315 Hz, c) 795 Hz, and d) 1245 Hz.

to Fig. 1.6. This is due to the directivity of the noise. Because plane 1 is closer to the source, the dominate region of sound radiation is further upstream along the angle of propagation. Also since plane 1 is closer to the source the peak SPLs are higher.

The spectral maps of the sound field at different engine powers confirm show similar frequency and distribution trends. In addition, the data provides evidence that the source moves upstream with decreasing engine power. The actual measured data from the F-22 is a huge resource and asset in trying to analyze and increase the understanding of full-scale jet noise.

Chapter 2

Model Development

2.1 Introduction

The purpose of this study is to explore the possibility of using a semi-empirical simple-source model as an equivalent source model for jet noise. The first section of this chapter with introduce the mathematical development of this model. It will include the equations necessary to employ the model and explanations to justify each step. The next section is an initial comparison between the model and the measured data and also points out how each component of the model contributes to the model's accuracy. To simplify, this initial application of the model only looks at one combination of frequency, measurement plane and engine condition. Additional data is analyzed in chapter 3.

2.2 Mathematical Development

To model the acoustic field for the jet plume, a collection of simple sources is used. A simple source is a single point source, also known as a monopole. A monopole radiates pressure omni-directionally, and the magnitude of the pressure falls off radially as a function of $\frac{1}{R}$. Explicitly, the

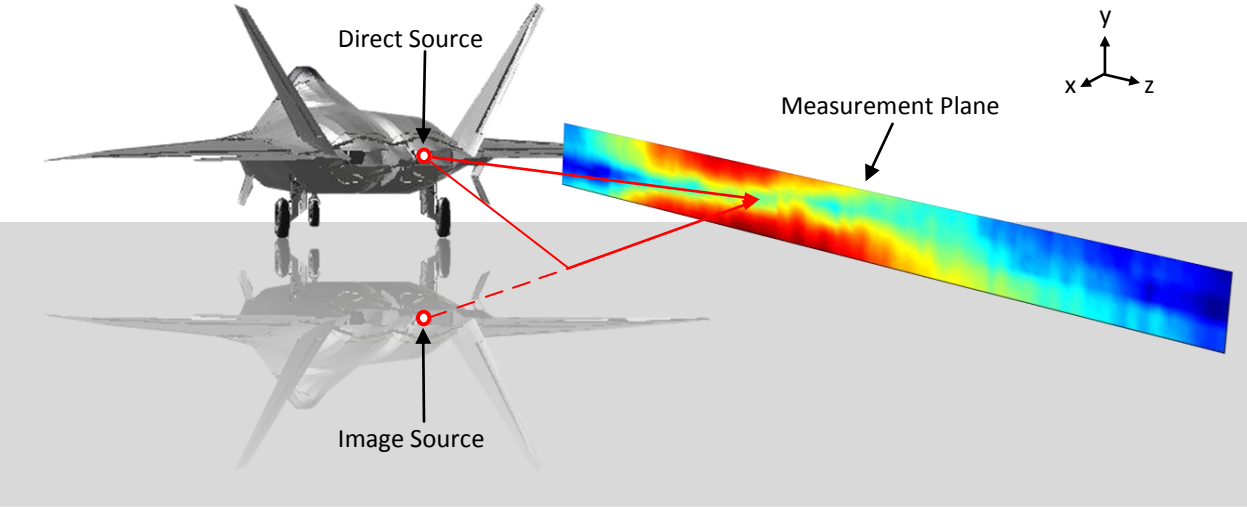

Figure 2.1 The relative location of the direct source, image source and measurement plane with respect to the jet's location.

complex pressure amplitude from a monopole is

$$\tilde{P} = \tilde{A}\frac{e^{-jkR}}{R} = \tilde{A}G(\vec{r},\vec{r}_o), \tag{2.1}$$

where $R = |\vec{r} - \vec{r}_o|$, k is the wavenumber for a given frequency and j is the complex number $\sqrt{-1}$. The Green's function, G, for a given frequency or k value is a function of the measured position vector, $\vec{r}$, and the source vector, $\vec{r}_o$. The origin for these vectors is set at the exit of the jet nozzle. The position of the monopole is adjustable within the jet plume with respect to the nozzle exist. Thus $\vec{r}_o$ is a variable source location and $\vec{r}$ is a matrix of locations corresponding to the measured data.

A key factor in applying the model is the interference patterns from the ground reflections, which are present in this type of experimental research since it requires that the jet be on the ground. Normally ground reflections are a nuisance in acoustical measurements because they interfere with the direct source radiation. For the case of this model, however, the interference patterns provide information about the position and distribution of the sources. The ground reflection creates a second source, known as the image source. Fig. 2.1 shows the location of the image source with

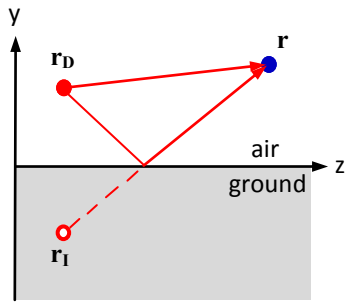

Figure 2.2 The ground reflection is modeled as an image source. The image source interferes with the direct source at the measurement location. The strength of the image source depends on the properties of the reflecting surface.

respect to the direct source in the jet plume and how they radiate to a measurement plane. Starting with the assumption that the source can be modeled as a monopole and its image, the total radiated pressure is

$$\tilde{P} = \tilde{A}[G(\vec{r},\vec{r_D}) + \tilde{Q}G(\vec{r},\vec{r_I})], \tag{2.2}$$

where $\vec{r}_D$ is the vector to the direct source and $\vec{r}_I$ is the vector to the image source. The relative amplitude and phase of the image source depends on $\tilde{Q}$, the spherical wave reflection coefficient, and on the properties of the ground. Absorptive grounds like snow and grass have small values of $\tilde{Q}$, while for rigid ground $\tilde{Q}$ is 1. Our experiment is on concrete which is a rigid surface, and thus setting $\tilde{Q}$ to be 1 is accurate for this study.

Eq. (2.2) gives pressure due to a single monopole with a ground reflection, a more reasonable representation of the noise source in the jet plume is a line array of monopole sources. This model will include an array of monopole sources with varying amplitudes. The total pressure from such an array is,

$$\tilde{P}_T = \sum_{m=1}^{N} \tilde{A}_m[G(\vec{r},\vec{r}_{D_m}) + \tilde{Q}_m G(\vec{r},\vec{r}_{I_m})]. \tag{2.3}$$

The pressure from each individual monopole is summed up over the index m from 1 to the total number of sources, N. This is the case for a correlated source. A correlated source is when each individual monopole in the source radiates at the same rate but with a set phase difference between

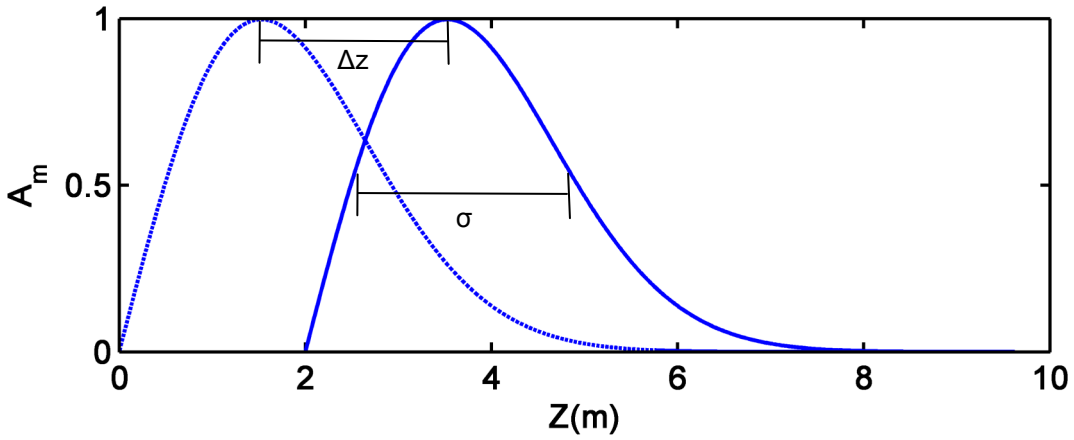

Figure 2.3 Example of a Rayleigh distribution, adjusted to have a peak amplitude of one.

each one as determined by the distance R in the Green's function.

The amplitude, $\tilde{A}_m$, is the relative amplitude for each monopole in the array. This amplitude distribution can be any shape as long as it has a peak amplitude somewhere in the distribution and decays off to zero at the ends. Possible distributions are a symmetric Gaussian distribution or an asymmetric Rayleigh distribution. Schlinker's research related in Figs. 10 and 13 of his paper supports an asymmetric distribution [4]. Studies on high-powered rockets also agree with an asymmetric distribution of amplitude sources [8]. One option for an asymmetric distribution is a Rayliegh distribution.

Based on a Rayleigh distribution, the amplitudes of the monopoles are

$$|\tilde{A}_m(z,\Delta z,\sigma)| = \frac{z_m-\Delta z}{\sigma} e^{\frac{-(z_m-\Delta z)}{2\sigma^2}} = A_m(z,\Delta z,\sigma), \tag{2.4}$$

where z_m is the location of the monopole, z is the peak amplitude location, Δz is the shift distance, and σ is the standard deviation of the distribution as shown in Fig. 2.3. The shift distance, Δz, is the change in z position necessary to move the peak distribution amplitude to the peak sound radiation location along the centerline of the jet. The peak amplitude is adjusted to always be 1. The Rayleigh distribution is asymmetric because the distribution rolls off more gradually in the

downstream z direction.

While the asymmetric Rayleigh distribution for monopole amplitudes match the observed source distribution within the jet plume, another consideration for the model is the fact that line array sources do not have to be perfectly correlated. According to Tam, jet noise is a mixture of correlated and uncorrelated sources [2]. For uncorrelated line array sources, each monopole radiates at random with respect to the others in the array. The total squared pressure from an uncorrelated source is the sum of the magnitude squared of the contributions of the direct and image source,

$$P_{T,u}^2 = \sum_{m=1}^{N} [A_m[G(\vec{r},\vec{r}_{D_m}) + \tilde{Q}_m G(\vec{r},\vec{r}_{I_m})]]^2. \tag{2.5}$$

The contribution of uncorrelated source in the model is included using squared pressures because this makes the total pressure real which has more physical value. This also makes it easier to add the uncorrelated and correlated source together to get the overall dB levels.

On the other hand not all sources are perfectly correlated. A correlated line array source really means that there is a set phase difference between each monopole source. This is like a time delay in the radiated pressure from each adjacent monopole. Correlated line arrays have several interesting acoustical properties and applications. A correlated line array is able to steer sound at an angle to the array instead of radiating equally in all directions. This is called, directivity, sound is focused in one direction from the source [2].

The correlated portions of the line array are responsible for the directivity of the sound radiation because the set phase difference between adjacent monopoles steers the sound at an angle θ relative to the array [2]. The phase difference is included in the amplitude of the line array. The amplitude distribution for each monopole, m, in a correlated source with a set phase difference is,

$$\tilde{A}_m(z,\Delta z,\sigma) = A_m(z,\Delta z,\sigma)e^{j\phi m}, \tag{2.6}$$

where d is the space between monopole sources and

$$\phi = \frac{2\pi f d sin(\theta)}{c}. \tag{2.7}$$

The far-field directivity angle, θ, comes from analyzing far-field data taken on an F-22 jet. The angle changes with engine power and frequency.

For correlated sources the total squared pressure is the sum of the individual monopole pressures with complex amplitude distributions squared. This gives the total squared pressure for the correlated source as

$$P_{T,c}^2 = [\sum_{m=1}^{N} \tilde{A}_m * [G(\vec{r}, \vec{r}_{D_m}) + \tilde{Q}_m * G(\vec{r}, \vec{r}_{I_m})]]^2. \tag{2.8}$$

There needs to be both a correlated and uncorrelated line array source in the model for jet noise. Each one has different contributions to the sound radiated to the measurement plane. Tam's two source model for jet noise indicates that uncorrelated, omni-directional sound comes from the FSS, whereas correlated, directional sound originates with the LSS [2].

Putting together both the correlated and uncorrelated components of the model for jet noise gives the total squared pressure:

$$P_T^2 = P_{T,c}^2 + P_{T,u}^2. \tag{2.9}$$

This total squared pressure is propagated, via the Green's function, to an observation point in the sound field. The observation points match up with the microphone positions for the measured data, such that the total pressure is calculated at each microphone location in a measurement plane. By this process the model generates a planar map of the sound field that is then compared to the measured data.

The model has several adjustable parameters: peak source location, width of line array amplitude distribution, relative amplitude between the two sources, type of distribution, spacing between sources and observation locations. These parameters are adjusted to yield the modeled results that match the primary features of the measured data.

2.3 Initial Application of Model

Because of the large number of parameters in the model, it is helpful to to show how each component of the model contributes to the total modeled field and to explain how each parameter of the model is chosen by comparing the model to the measured data. This section addresses one frequency - 315 Hz, one engine power - afterburner, and propagate to one measurement plane namely, plane 2.

The most basic component of the model is the combination of the direct source with the image source as expressed in Eq. (2.2). The adjustable parameters of this equation are $\vec{r}_D$ and $\vec{r}_I$, which are functions of x, y, and z. For $\vec{r}_D$ and $\vec{r}_I$, the direct sources are on the centerline of the jet so x is zero, y is the height of the nozzle from the ground, 1.9 m and z is the distance downstream and for the image source y is -1.9 m below ground. Thus, both x and y are fixed values while z is an adjustable parameter.

Figure 2.4 shows the results of Eq. (2.2) of the model when a single direct source and its image are used compared to the measured data. The z parameter is adjusted until the location of null in the model matches the null in the measured data. The null is the large decrease in sound pressure level (SPL) caused by destructive interference between direct and image source. Fig. 2.4 part a) shows the results when z is far downstream, part b) is when z is at three m, part c) is when z is near the nozzle, and part d) is the measured data. By comparing parts (a) to (c) that location of the null in the model best fits the measured data when z is at three meters downstream of the nozzle.

It can be seen from Fig. reffig:point that the two interfering monopole sources are not a good representation of jet noise and are only able to predict the location of the null from the ground reflection. While the z in Fig. 2.4 is the location of a single direct source and its image, the best value of z = three meters is used in calculating Δz in the Rayleigh distribution, Eq. (2.4).

The contributions from the rest of the components of the model outlined in section 1.3, are shown in Fig. 2.5. Fig. 2.5 (a) again shows the location of the null from the interference of a single

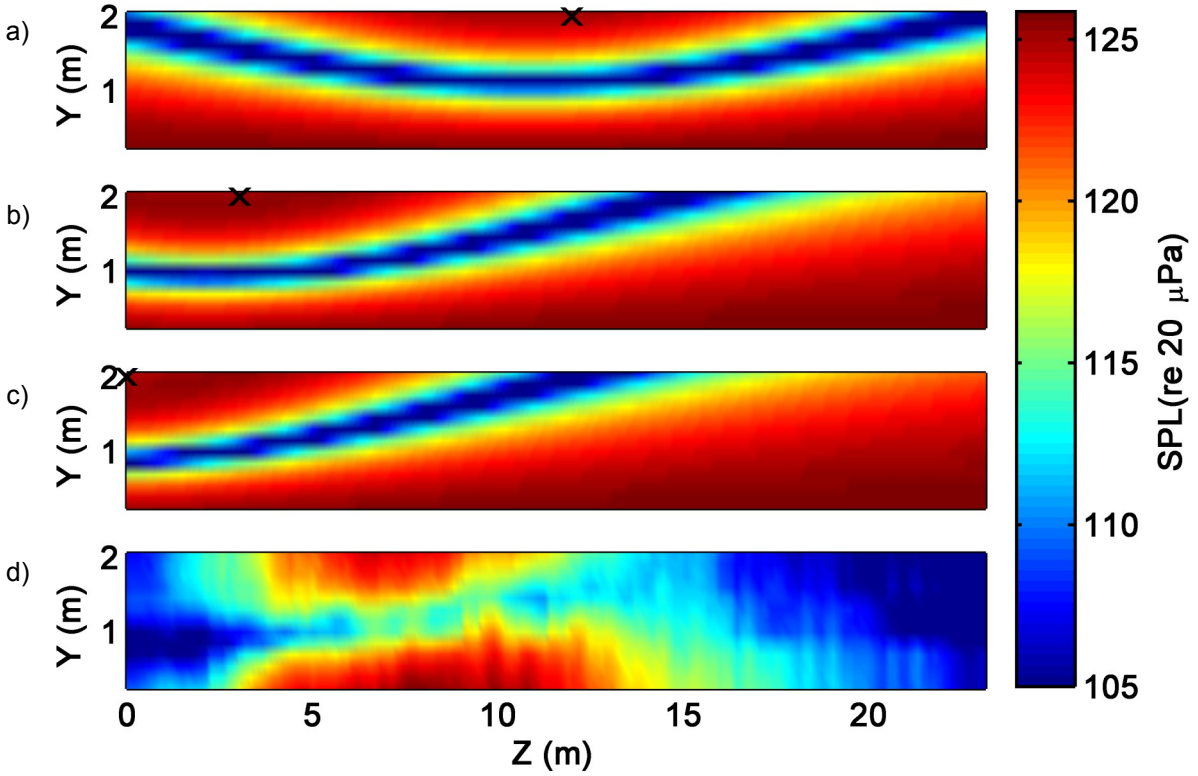

Figure 2.4 This is the case of 315 Hz at afterburner condition with the first three plots being a single point source with its image source at different distances downstream: a) z is 10 m, b) z is 0 m, and c) z is 3 m. Part d) is the measured data. Having the point source at 3 m is the best match between the model's null and the measured data.

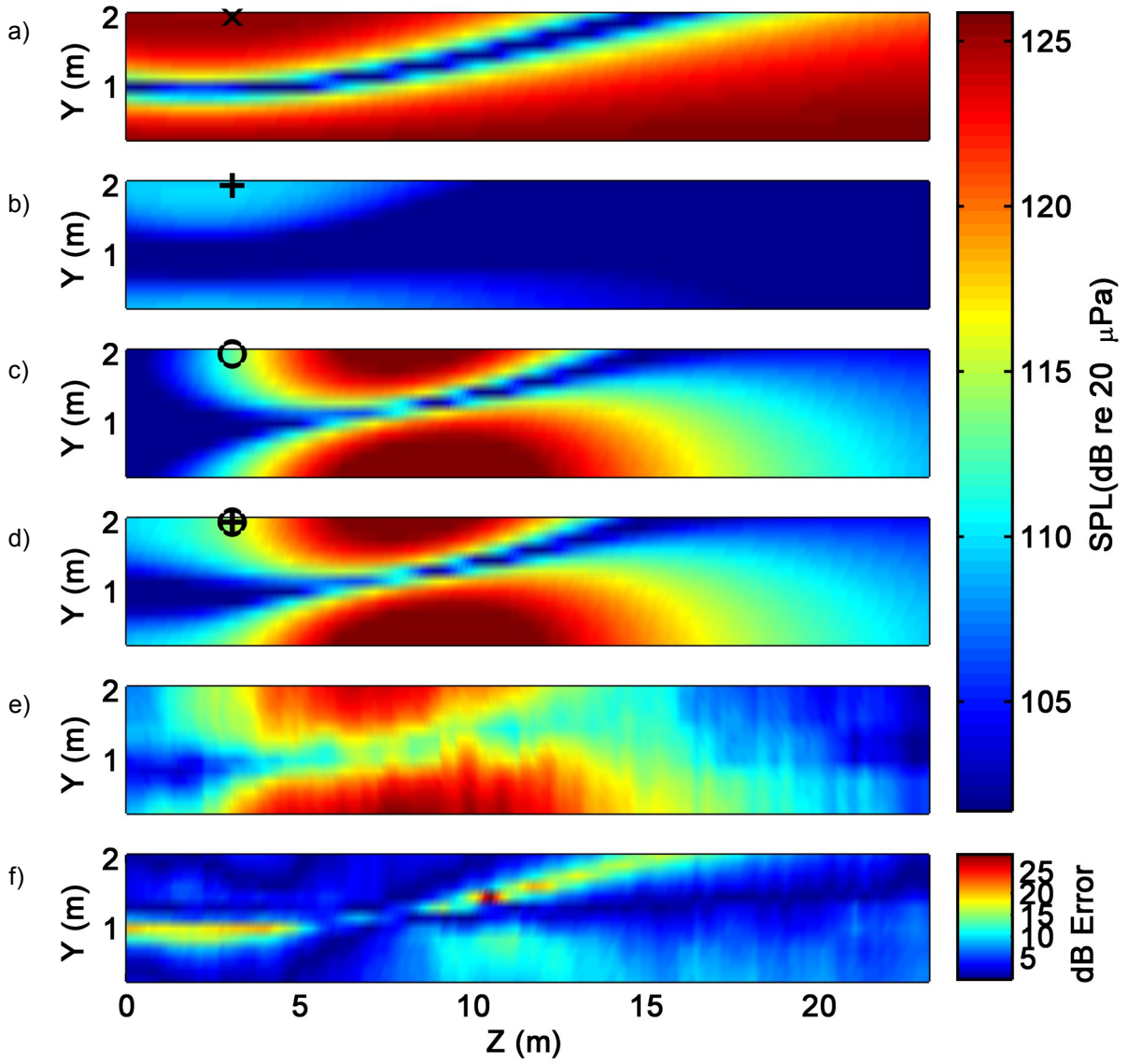

Figure 2.5 The different components of the model and measured data at 315 Hz and afterburner engine condition with the peak source location at 3 m: a) direct source interfering with the image source, b) uncorrelated source, c) correlated source, d) two source model: uncorrelated and correlated sources, e) measured data, f) dB error between d) and e).

direct source and image source with z equals three meters. The entire plane has a constant SPL level except for the null. The remaining parts of Fig. (2.5) show the different pieces of the model and how they fit together to approach the data.

Figure 2.5 (b) is the sound map for an uncorrelated line array source from Eq. (2.5) with the Rayleigh distribution, Eq. (2.4) used to determine the amplitude distribution. The spacing, d, between the monopoles in the line array is small in order to simulate a continuous source. The uncorrelated source broadens the nulls so that the radiated sound is focused around the peak source location. It contributes mostly to the sideline radiation, the sound radiated to the upstream side of the jet plume. Alone the uncorrelated line array does not match the measured data.

Figure 2.5 (c) is the sound map for just the correlated line array source from Eq. (2.8). Again the spacing, d, is small to simulate a continuous source and improves the focus of the radiated sound from the correlated line array into one direction. The ϕ is chosen according to known experimental far-field directivity patterns. The ϕ is a function of the frequency and the engine power. At 315 Hz, the afterburner engine power has a measured far-field directivity angle, ϕ, of 125 degrees from the aft of the jet with the nozzle as the center of the axis. For this frequency, the correlated source contributes most of the radiated sound in the downstream direction. This is the dominate source, but it is not a prefect match to the measured data.

Figure 2.5 (d) shows the radiation pattern using a combination of the correlated and uncorrelated sources in the model. Adding the uncorrelated source to the correlated source improves the model so that it better matches the measured data shown in Fig. 2.5(e). Specifically, the uncorrelated sources increase the radiated sound in the upstream direction and decreases the depth of the null from the correlated source. When both sources are added together the best match is found between the model and measured data. Thus, the combination of uncorrelated and correlated line array sources capture the primary features of the data and correspond with the two source model for jet noise [9].

Figure 2.5 (f) is the dB error between parts (d) and (e). The dB error is defined as the absolute value of the model's SPL minus the measured data's SPL. Areas of low dB error are in blue. The red areas, areas of least agreement, are aligned with the nulls. Although the model predicts that the nulls are deeper than they really are there is still good agreement between the model and measured data. The map of the dB error is a visual assessment of the error.

A quantitative method of measuring total error is to average the error on a point-by-point basis between the model and measured data. The total error is calculated by

$$Error = 10\log_{10}\left(\frac{\sum_{i=1}^{\tilde{N}} |\tilde{P}_{r,i}^2 - \tilde{P}_{m,i}^2|}{\sum_{i=1}^{\tilde{N}} \tilde{P}_{r,i}^2}\right), \tag{2.10}$$

where $\tilde{P}_r$ is the reference pressure from the measured data and $\tilde{P}_m$ is the model calculated pressure [10]. Since it is on a log scale, the set of parameters with the largest negative value has the least error. The disagreement between the depth of the nulls in the measured data and the model is the greatest contributor to the total error. To reduce the null contribution and focus on agreement between the peak values only SPL values within 10 dB of the peak measured SPL are included in the error calculation, where $\tilde{N}$ are only the points with this 10 dB range. There are multiple parameters to adjust to attempt to get the lowest possible error value. One of those is the distribution of the source amplitudes.

The actual amplitude distribution may not follow a set distribution function like the Rayleigh distribution. The Rayleigh distribution is just used as a good approximation. To further justify the use of an asymmetric Rayleigh distribution compared to a symmetric Gaussian, Fig. 2.6 shows the model results for each distributions compared to the measured data. Fig. 2.6 (a) is the model with a Gaussian distribution. Fig. 2.6 (b) is the model with a Rayleigh distribution. The results using a Rayleigh distribution better reflects the shape of the measured data. In the Gaussian distribution plot, the high amplitude SPL levels decay more slowly in the downstream direction while in

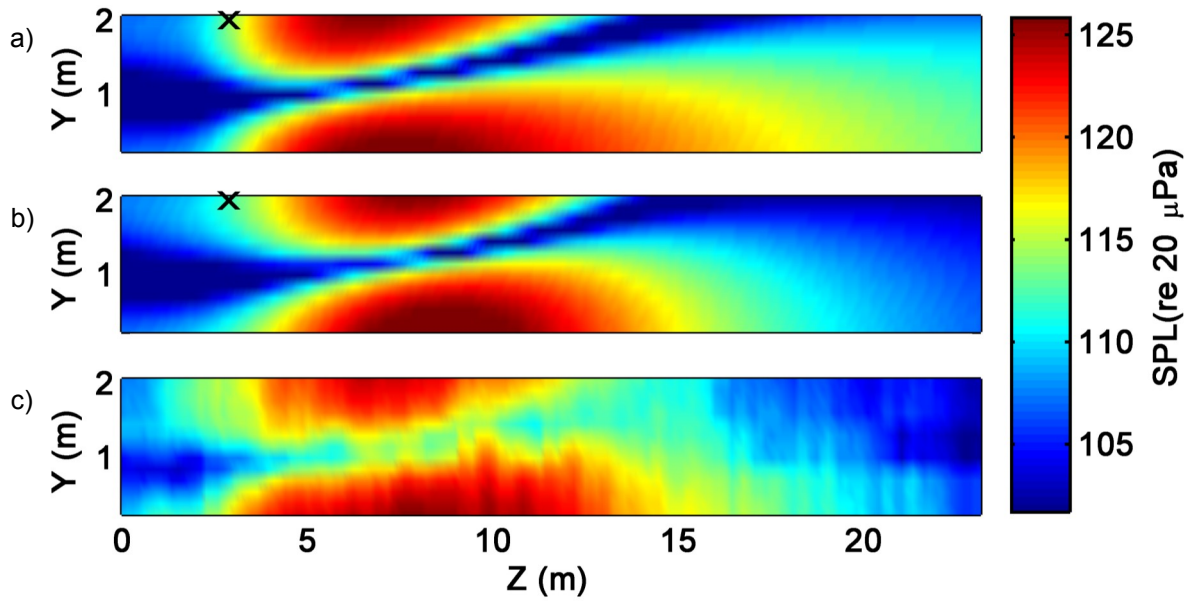

Figure 2.6 Comparing the model with two different source amplitude distributions: a) Gaussian distribution, b) Rayleigh distribution and c) is measured data.

both the Rayleigh distribution plot and measured data the same high amplitude SPL levels drop off at the same downstream position. The Rayleigh distribution plot is a closer match to the information in the upstream direction of the measured data than the Gaussian distribution plot. The Rayleigh distribution is better for the model but not necessarily the only option for an asymmetric distribution.

Overall the model proves to be a capable equivalent source model for jet noise. It can predict levels and SPL distributions in a measurement plane. This section has described only a single example of applying the model to measured data. The model needs to be able to apply to other frequencies, measurement planes and engine powers.

Chapter 3

Results and Discussion

3.1 Model Results

The previous chapter outlines the mathematical development and initial application of a semi-empirical simple source model as an equivalent source for jet noise. The initial application of the model only covered one set of conditions: 315 Hz, afterburner engine power and propagating to measurement plane 2. For the model to be more applicable it needs to be accurate for other parameters. This section of the chapter focuses on changing the propagating distance, the frequency and the engine power.

3.1.1 Benchmark Tests

To test the model at different distances a series of benchmark tests will be done. A benchmark is a reference point. Measurement planes 4 and 1 are good benchmarks tests to access the accuracy of the model at distances closer to and further away from the jet plume than plane 2. The data from measurement plane 2 is used to pick the model parameters. At plane 2, the model is able to recreate the general shape and amplitude of the jet noise. The set of model parameters that work

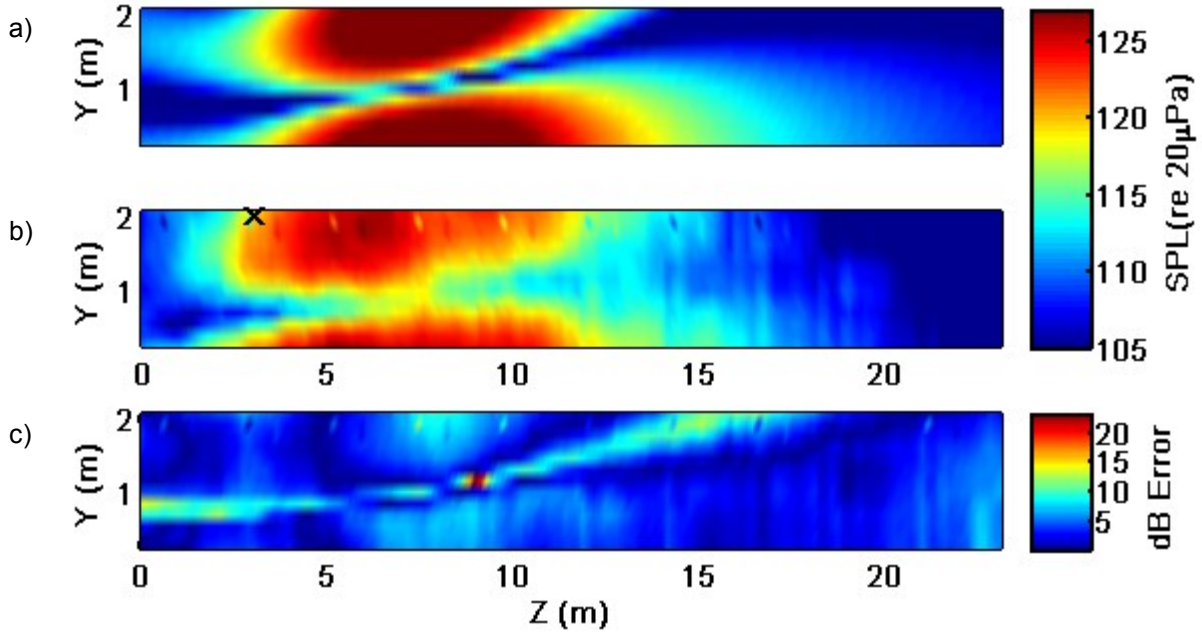

Figure 3.1 At measurement plane 1, 3.8 m from shear layer where a) model, b) measured data and c) dB error.

for plane 2 need to work and apply at the other distances as well.

Figure 1.5 is an overview of the experimental set up showing the position of planes 1 and 4 relative to plane 2. As Fig. 1.5 shows that plane 1 is parallel to plane 2 except closer to the jet plume while plane 4 is an arc spaced out in 10 degree increments a set distance away. One of the benchmark tests is closer and the other further away which is best for testing the overall application of the model.

As mentioned, plane 1 is parallel to plane 2, but closer to the shear layer of the jet plume at only 3.8 m away instead of 5.6 m. The source distribution, location and amplitude for the case of 315 Hz at afterburner is empirically based on plane 2 measurements. Fig. 3.1 is for the exact same source and conditions, but instead propagated to plane 1. In Fig. 3.1 (b) the measured data has a repeated anomaly from a single bad microphone at the top of the measurement, but this does not effect the accuracy of the model. Mathematically, for the model, Green's function only

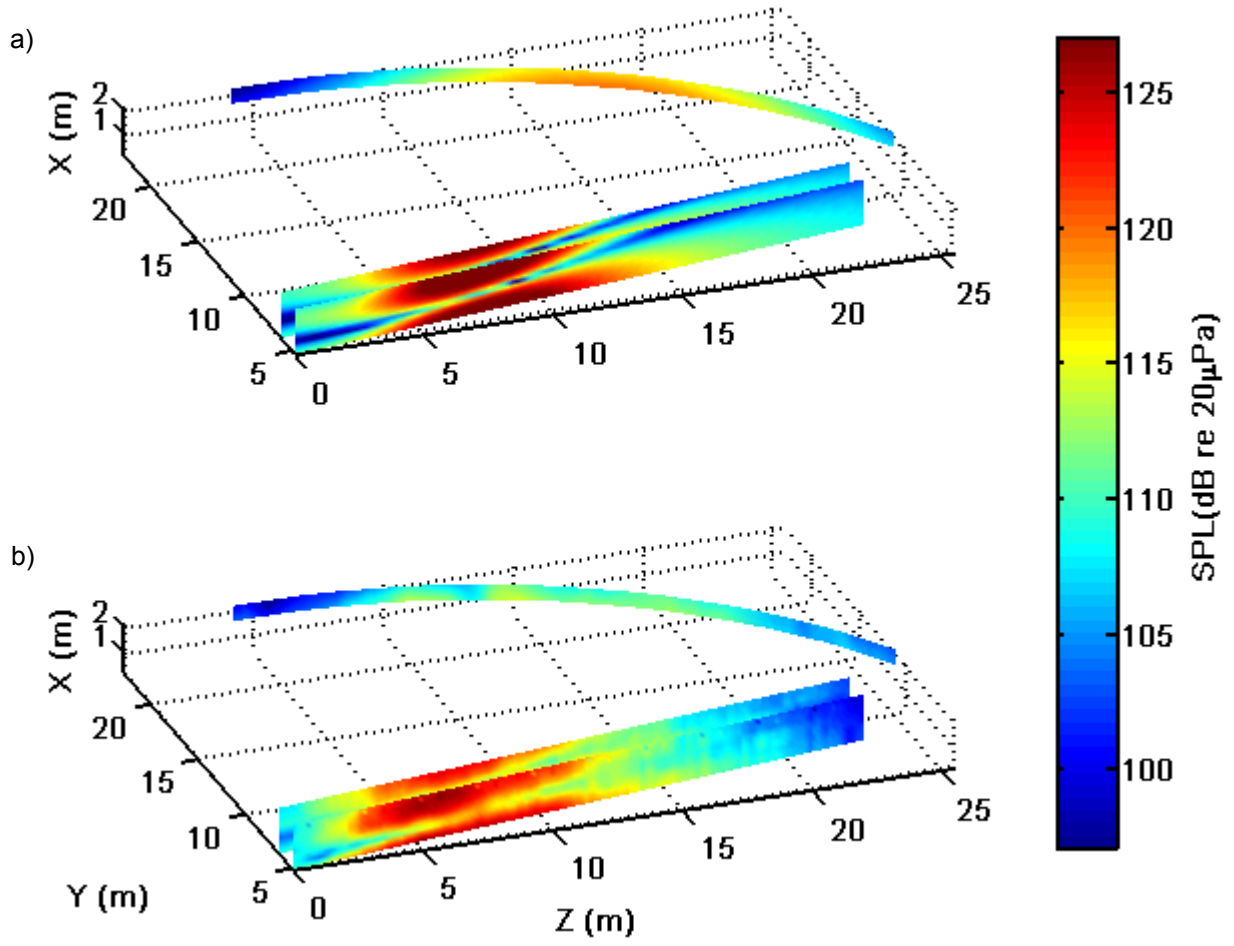

Figure 3.2 A 3-D plot to show multiple measurement planes and agreement between model and data at various distances: a) model and b) measured data.

changes in the values of $\vec{r}$ by changing the propagation distance. Fig. 3.1 shows that there is the same agreement at plane 1 as at plane 2 shown in Fig. 2.5. The model has the general shape and amplitude of the sound. Thus this model is capable of reconstructing measurement planes that are closer to the jet plume than the original reference plane. Other purely computational methods of analyzing the source, such as NAH, have difficulty in propagating in towards the source due to decaying evanescent waves. Most models are more capable of propagating outward to further distances until atmospheric absorption takes too big a toll on the SPL.

The model also needs to be able to reproduce measurement planes that are further from the source. The other plane of interest is measurement plane 4, which is the arc of data in 10 degree increments 22.9 meters away from the peak source location of the jet plume. For other analytical methods propagates further out is simpler, but for the model this is a much larger distance and any errors in the construction of the source at plane 2 could be emphasized. This arc as plane 4 is useful for checking the directivity of the model's source. The best way to show the comparison between the model and measured data for this plane is in a 3-D plot. Fig. 3.2 shows all three measurement planes: plane 1, plane 2 and plane 4. Fig. 3.2 (a) is the model's reconstruction of (b) the measured data. Looking at the arc in Fig. 3.2, the amplitude of the sound rolls off correctly in both the upstream and downstream directions. The peak source area agrees with the angle of the known far-field directivity pattern for the afterburner engine condition of 125 degrees from the aft of the aircraft. The simple-source model proves capable of reproducing the measured jet noise at any distance away from the source. This provides accuracy and flexibility in the model.

3.1.2 Other Frequencies

The model is accurate for at least one frequency, but jet noise contains a large range of frequencies. So the model needs to work for multiple frequencies. This section will show the model at two different frequencies: one lower and one higher than 315 Hz for simplicity at measurement plane 2 and afterburner engine condition. The parameters of the source depend on frequency since Green's function shown in Eq. (2.5) and Eq. (2.8) is frequency dependent. The source distribution, location, and amplitude varies for each frequency.

A reasonable higher frequency to look at is 795 Hz. Fig. 3.3 is 795 Hz at plane 2 and afterburner engine condition where (a) is the model, (b) measured data and (c) dB error. This frequency has multiple nulls intersecting the measurement plane. This is due to its shorter wavelength which decreases the distance between nulls. Fig. 3.3 shows that the model can reproduce each one of

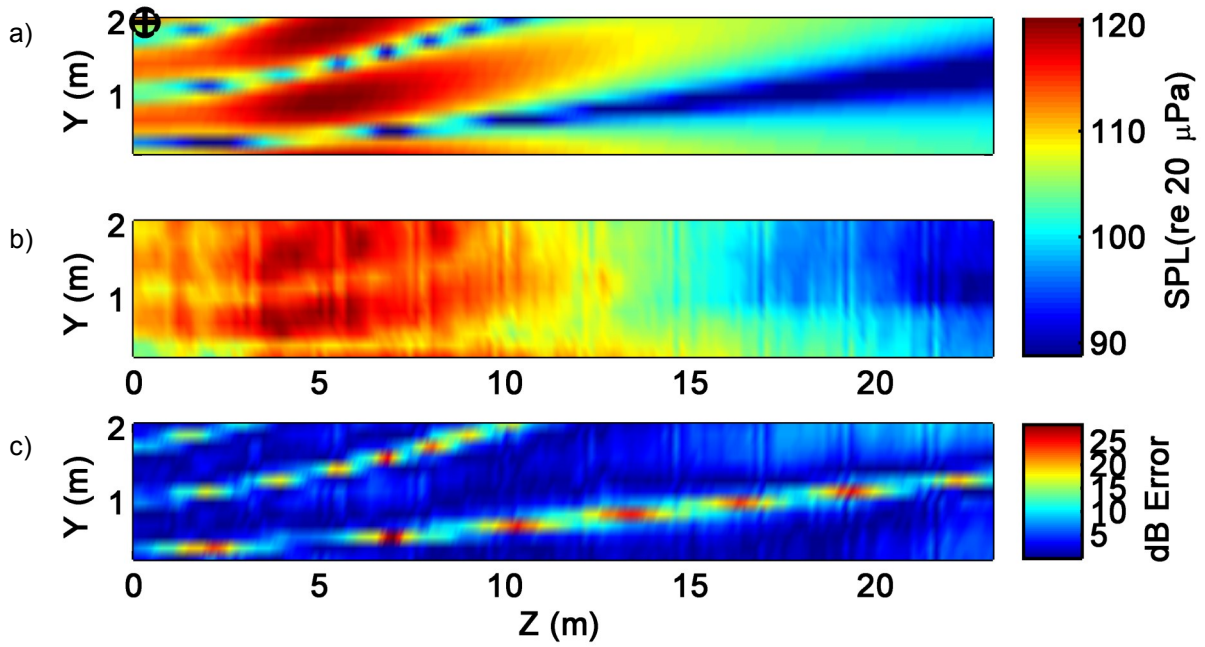

Figure 3.3 At measurement plane 2 for 795 Hz with z = .3 m, a) model, b) measured data and c) dB error.

these nulls and their respective locations and shapes. The peak source location for this higher frequency is .3 m downstream. This is just off the nozzle of the aircraft. In comparing Fig. 3.3 and Fig. 2.5, it is visibly noticeable that the peak amplitude region in the measurement plane moves upstream with increasing frequency.

On the other end of the spectrum, Fig. 3.4 is 150 Hz at plane 2 and afterburner engine condition. This frequency is low enough that there are no nulls in the measurement plane. The measured data in Fig. 3.4 (b) has a half circle shape. Fig. 3.4 shows that the model is still able to produce this different feature. Just as the higher frequency is upstream from 315 Hz, the lower frequency is further downstream. In the model, the peak source location is about 6 m downstream. This is near the overall dominate source location since about 125 Hz is the frequency that produces the peak amplitude sound.

The movement of the peak source location agrees with the theory and other experiments.

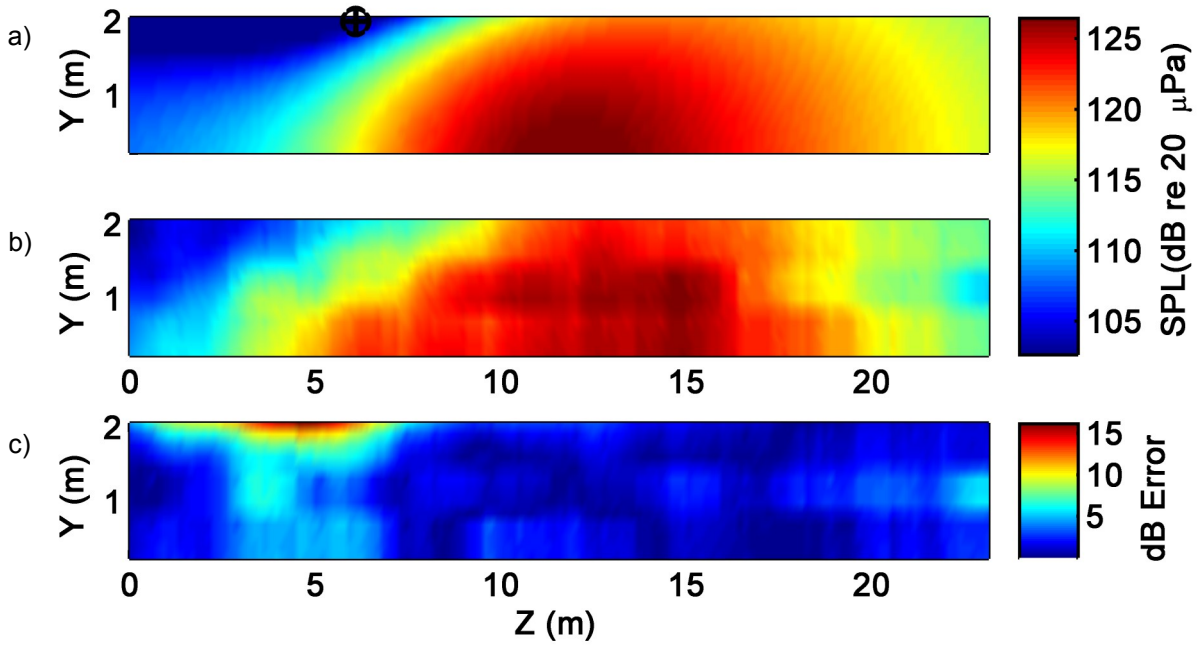

Figure 3.4 At measurement plane 2 for 150 Hz with z = 6 m, a) model, b) measured data and c) dB error.

Schlinker's research on supersonic jets shows an exponential trend of peak source locations moving upstream with higher frequency [4]. The model agrees with this with higher frequencies close to the nozzle and lower frequencies spread out downstream. The turbulence structures in the jet plume cause the noise. FSS form right out of the nozzle and cause high frequency noise. The turbulence structures grow and spread out as they move downstream resulting in large turbulence structures downstream that cause low frequency noise. The model captures this physical system. Overall the model works over a distribution of frequencies.

3.1.3 Other Engine Powers

The next case variable to explore is the adjustment of the engine power. This section will hold 315 Hz at measurement plane 2 constant and adjust the engine power. There are four different engine powers: idle, intermediate, military and afterburner. Idle is the least powerful and very

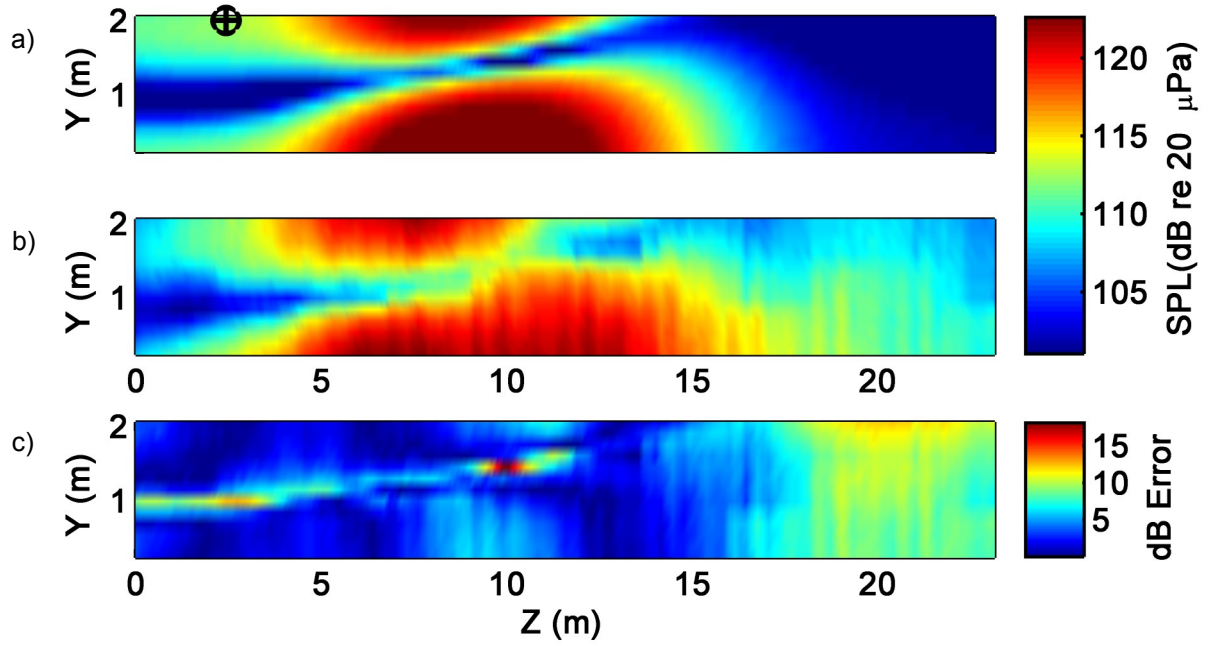

Figure 3.5 At measurement plane 2 for 315 Hz at military engine condition with z = 2.4 m, a) model, b) measured data and c) dB error.

similar to the intermediate engine power. Afterburner is the most powerful and propels the aircraft to supersonic speeds. Military engine power is between the two extremes, closer to the afterburner engine condition.

Figure 3.5 is 315 Hz at plane 2 and military engine power with (a) model, (b) measured data and (c) dB error. The measured data in Fig. 3.5 (b) and Fig. 2.5 (e) have similar shapes and distributions, but the military case is several dB lower and the peak amplitude area cuts off sooner and is further upstream. Since the military engine power is not as powerful, the jet plume is not as long and is more concentrated upstream. The peak source location for the military engine power is 2.4 m while afterburner is 3 m. The peak source location moves upstream with decreasing engine power.

Fig. 3.6 shows the model at the idle engine power. The intermediate engine power is very similar and would be repetitive to show explicitly. Fig. 3.6 shows that the peak source location

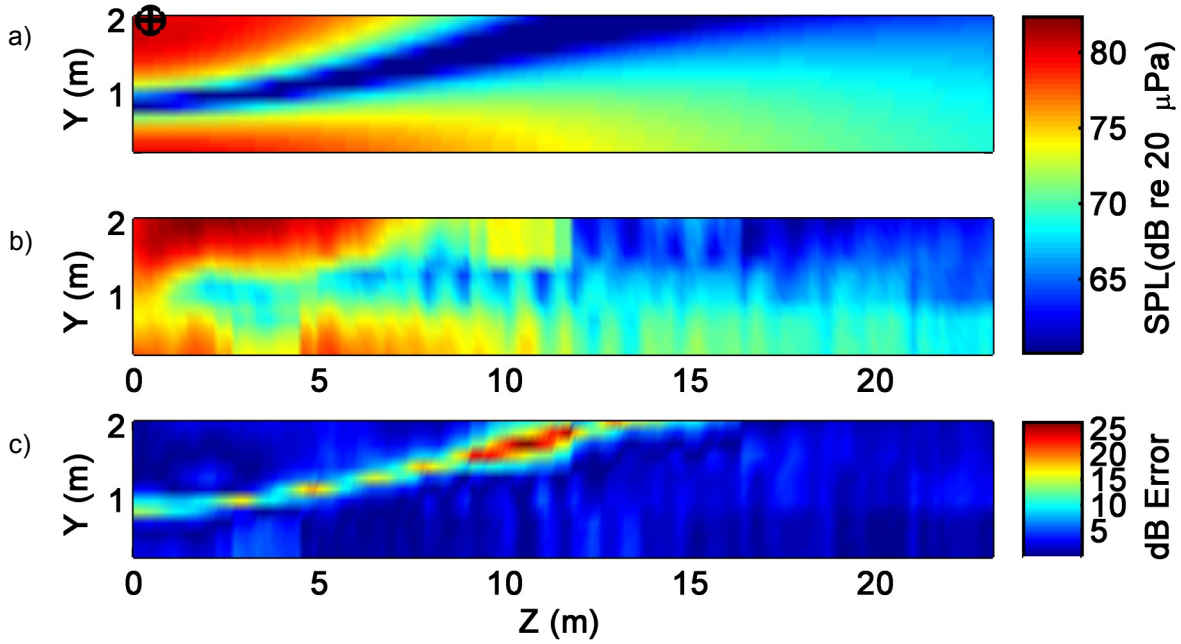

Figure 3.6 At measurement plane 2 for 315 Hz at idle engine condition with z = 0.5 m, a) model, b) measured data and c) dB error.

is very close to the nozzle and focused mostly as sideline radiation. The SPL levels are much lower for this condition reflecting the lower engine power. This equivalent model for this set of conditions contains little to none correlated line array information. This model consists mostly of just uncorrelated line array sources which produces the sideline radiation seen in the data. This model captures the theory's prediction for lower peak amplitude, for the source being near the nozzle and mostly containing mostly sideline radiation.

Overall the engine powers have similar distribution trends with the changing frequencies as seen in the AB case. The peak source location moves upstream with decreasing engine power. This is due to the decrease in jet velocity at lower engine conditions so the LSS does not have a chance to grow and develop downstream. These results show that the model is able to accurately account for changing engine powers.

3.2 Conclusions and Future Outlook

The model is able to make an equivalent source of jet noise in various scenarios including engine conditions, frequency and measurement plane to recreate measured data. The equivalent source is useful in understanding jet noise sources. This simple source model incorporates all the major characteristics known for jet noise theory.

The equivalent sources in the model conclude that the peak source location moves upstream exponentially as frequency increases. Similarly, the peak source location moves upstream with lower engine powers. The relative amplitudes of the correlated and uncorrelated line array sources vary with each combination of frequency and engine power. For high engine powers and low frequencies the correlated line array source dominates. Whereas for low frequencies especially at low engine powers the uncorrelated line array source is the dominate source. Both line array sources are necessary in order for the model to be accurate and apply to a larger set of cases. The necessity of both line arrays makes it so that the model is a two source model consistent with Tam's two source theory of jet noise [2].

The model does have slight flaws such as the overestimation of the depth of the nulls, different combinations of parameters producing similar plots, and the time it takes to explore all the different parameter options. The model assumes that the only sources of sound are the point sources located on the center line of the jet plume and that they all reflect perfectly with the ground. A possible addition to the model is a third random volume source that does not reflect off the ground. This will simulate the more chaotic nature of the jet plume resulting in not all the sound reflecting perfectly. This will decrease the depth of the nulls and therefore decrease the error of the model.

The entire model can be made into a mathematical inverse problem. This new method will optimize the entire process. The computer will run through all the different combinations of parameters and pick the one with the least error. This reduces the amount of human error that is present even with the current error calculation. The mathematical inverse method would also have

the capability of producing the amplitude distribution with the best fit to the data instead of pre-set distribution. This would give the actual source distributions. This method will also improve the efficiency of the model. The goal is that once the model is made into a mathematical inverse problem it can be applied like NAH or Beamforming to analyze jet noise sources.

Bibliography

[1] G. M. Lilley, in *Aeroacoustics of Flight Vehicles-Theory and Practice*, H. H. Hubbard, ed., (1995), Vol. 1.

[2] C. K. W. Tam, K. Viswanathan, K. K. Ahuja, and J. Panda, "The sources of jet noise: experimental evidence," J, Fluid Mech. **615,** 253–292 (2008).

[3] D. Papamoschou, *Imaging of Directional Distributed Noise Sources* (2008).

[4] R. H. Schlinker, S. A. Lijenberg, D. R. Polak, K. A. Post, C. T. Chipman, and A. M. Stern, *Supersonic Jet Noise Source Characteristics and Propagation: Engine and Model Scale* (2007).

[5] S. S. Lee and J. Bridges, *Phased-Array Measurements of Single Flow Hot Jets* (2005).

[6] C. K. W. Tam, "Jet Noise: Since 1952," Theoret. Comput. Fluid Dynamics **10,** 393–405 (1998).

[7] F. Holste, "An Equivalent Source Method For Calculation of the Sound Radiated From Aircraft Engines," J. Sound Vibr. **203,** 667–695 (1997).

[8] J. Haynes and R. J. Kenny, *Modifications to the NASA SP-8072 Distributed Source Method II for ARes I Lift-off Environment Predictions* (2009).

[9] C. K. W. Tam, N. N. Pastouchenko, and R. H. Schlinker, "Noise source distribution in supersonic jets," J. Sound Vibr. **291,** 192–201 (2006).

[10] J. Hald, "Basic Theory and Properties of Statistically Optimized Near-Field Acoustical Holography," J. Acoust. Soc. Am. **124,** 2105–21020 (2009).

[11] J. P. T.F.W. Embleton and N. Olson, "Outdoor sound propagatoin over ground of finity impedance," J. Acoust. Soc. Am. **59,** 267–277 (1976).

Index